Journal of Statistical Physics, Vol. 82, Nos. 5/6, 1996

Chronotopic Lyapunov Analysis. I. A Detailed Characterization of 1D Systems

Stefano Lepri,[1] Antonio Politi,[2] and Alessandro Torcini[3]

Received April 24, 1995; final August 1, 1995

Instabilities in 1D spatially extended systems are studied with the aid of both temporal and spatial Lyapunov exponents. A suitable representation of the spectra allows a compact description of all the possible disturbances in tangent space. The analysis is carried out for chaotic and periodic spatiotemporal patterns. Singularities of the spectra and localization properties of the associated Lyapunov vectors are discussed.

KEY WORDS: High-dimensional chaos; spatiotemporal instabilities; temporal and spatial Lyapunov spectra; coupled map lattices, localization.

1. INTRODUCTION

Linear stability analysis of chaotic dynamics is usually concerned with the problem of measuring the divergence of nearby trajectories.[1] In extended systems, the spatial dependence of the state variable requires considering also propagation phenomena and, more generally, spatial inhomogeneities.[2] The full characterization of a generic perturbation involves both its temporal and spatial growth rates as complementary measures of its instability properties. Two classes of Lyapunov exponents have been separately introduced for this purpose: the former aims at describing the temporal evolution of disturbances with an exponential profile in space;[3] the latter deals with the spatial shape of a perturbation defined on a given site at all times.[4]

[1] Dipartimento di Fisica, Universitá di Bologna, and Istituto Nazionale di Fisica Nucleare, I-40127 Bologna, Italy.
[2] Istituto Nazionale di Ottica and Istituto Nazionale di Fisica Nucleare, I-50125 Firenze, Italy.
[3] Theoretische Physik, Bergische Universität-Gesamthochshule Wuppertal, D-42097 Wuppertal, Germany.

0022-4715/96/0300-1429$09.50/0

These, which will be called *temporal* and *spatial* exponents, represent the starting point of this paper. Their definitions are given in Section 3.

Other indicators have been introduced in the attempt to characterizing the mechanisms of information transport. In this case, the object of study is the propagation of initially localized disturbances and has led to the introduction of the comoving Lyapunov exponents.[5,6] Moreover, the Lyapunov analysis of a given $(1+1)$D pattern can, in principle, be carried out along any direction. In fact, by performing a spatiotemporal rotation, i.e., by combining the role of space and time, it is possible to define still another class of "rotated" exponents.[7]

It has been shown that the maximum comoving Lyapunov exponent can be obtained from the maximum temporal exponent through a Legendre transform.[3] Moreover, the Kolmogorov–Sinai entropy turns out to be independent of the propagation direction along a spatiotemporal pattern.[7] Therefore, there must exist strong relationships among the several classes of exponents so far introduced. A particularly appealing problem is that of identifying the independent indicators which are necessary and sufficient for a complete characterization of a linear instability.

The present work, divided into two parts, intends to represent a first step toward a general and coherent theory. In this first part, we start from the observation that the most general perturbation is identified by two rates λ, μ describing its growth in time and space, respectively. The number of linearly independent perturbations can be expressed by two integrated densities, $n_\lambda(\mu, \lambda)$ and $n_\mu(\mu, \lambda)$. They provide a dual representation of the problem since any perturbation is unambiguously identified by the pair (n_μ, n_λ) as well as by (μ, λ). The properties of these indicators are studied in several models of coupled map lattices (CML), since we are confident that the tools and the results apply equally well to systems with continuous space and time variables. The relationship with the indicators arising from reference-frame-dependent analysis of disturbances will be thoroughly discussed in the second part.[8]

In Section 2 several classes of CML models are recalled, which have been designed to mimic reaction-diffusion systems, many-degrees-of-freedom Hamiltonian dynamics, and systems with a conserved order parameter. As already anticipated, in Section 3 spatial and temporal spectra are formally defined. In Section 4 we introduce the so-called (μ, λ) plane, which provides a compact graphical representation of Lyapunov spectra. It also allows enlightening analogies and differences between spatial and temporal exponents.

CML Lyapunov analysis has several analogies with the Schrödinger problem in disordered lattice systems.[4,9] This allows us to extract from the spatial spectra information about the localization of the temporal

Lyapunov vectors, thus confirming the close relationship between the two approaches. A discussion of the analogies with the Anderson tight-binding problems is presented in Section 5, where the the (μ, λ) representation is used for a straightforward identification of exponentially localized vectors. Moreover, the presence of singularities in the spatial Lyapunov spectrum is interpreted as a stretched-exponential behavior of the vectors. Finally, another type of singularity occurring in the temporal spectrum is illustrated. Some general remarks introducing the reader to the second part are presented in Section 6.

2. 1D MODELS FOR EXTENDED SYSTEMS

Spatiotemporal chaos and instabilities in extended systems have been widely studied with the aid of simplified models of reaction-diffusion processes, whose 1D form is of the type[2]

$$\partial_t \mathbf{y} = \mathbf{F}(\mathbf{y}) + \mathbf{D}\partial_x^2 \mathbf{y} \tag{1}$$

where the state variable $\mathbf{y}(x, t)$ is a vector defined on the domain $[0, L]$ [periodic boundary conditions $\mathbf{y}(0, t) = \mathbf{y}(L, t)$ are generally assumed]. The nonlinear function $\mathbf{F}$ accounts for the local reaction dynamics, while the diffusion matrix $\mathbf{D}$ represents the strength of the spatial coupling of the different $\mathbf{y}$ components.

Unfortunately, accurate numerical investigations of partial differential equations like (1) can require very long CPU times even on powerful computers. The introduction of simpler models, such as chains of coupled oscillators, can be already of great help for understanding the statistical properties of spatiotemporal chaos. An even simpler class of systems is obtained by assuming both time and space variables as discrete, i.e., by considering CML. The most natural updating scheme is

$$y_{n+1}^i = F(y_n^i) + (1-\varepsilon)\, y_n^i + \frac{\varepsilon}{2}(y_n^{i+1} + y_n^{i-1}) \tag{2}$$

where, for the sake of simplicity, y is now assumed to be a scalar variable. The indexes i, n label space and time directions, respectively, while ε gauges the diffusion strength. Model (2) has some technical limitations since, for arbitrary F, it leads to diverging solutions. To avoid such difficulties one can postulate a CML dynamics of the form[10, 11]

$$y_{n+1}^i = f\left((1-\varepsilon)\, y_n^i + \frac{\varepsilon}{2}[\, y_n^{i-1} + y_n^{i+1}]\right) \tag{3}$$

where f is a nonlinear function mapping a given interval I of the real axis onto itself. Periodic boundary conditions $y_n^{i+L} = y_n^i$ are again assumed. A generalization of model (3) has been proposed[5] to study convective instabilities, namely

$$y_{n+1}^i = f((1-\varepsilon)\, y_n^i + \varepsilon[(1-\alpha)\, y_n^{i-1} + \alpha y_n^{i+1}]) \tag{4}$$

The parameter α (comprised between 0 and 1) accounts for the possibility of an asymmetric coupling, mimicking open-flow systems (first-order derivatives in the continuum limit). Obviously, the symmetric case (3) is recovered for $\alpha = 1/2$.

Coupled maps are sometimes used also as test ground for extended Hamiltonian systems. The corresponding models are generally formulated in such a way that the evolution in tangent space is described by symplectic matrices. As a specific example we will refer to the coupled-standard-map lattice[12]

$$\begin{aligned} p_{n+1}^i &= p_n^i - k\left[\sin q_n^i + \frac{\varepsilon}{2}\sin(q_n^{i+1} - q_n^i) + \frac{\varepsilon}{2}\sin(q_n^{i-1} - q_n^i)\right] \\ q_{n+1}^i &= q_n^i + p_{n+1}^i \pmod{2\pi} \end{aligned} \tag{5}$$

where the parameter k rules the amplitude of the nonlinear coupling.

Finally, there is a last class of models that has been used to study evolution in the presence of a conserved order parameter.[13] Such CML models have been introduced in order to make a closer contact with the dynamics of microscopic conserved dynamical variables in strongly turbulent fluids. A general scheme for constructing a CML with a conserved quantity is to impose that $y_{n+1}^i - y_n^i$ is written as a spatial gradient. For example,

$$y_{n+1}^i = y_n^i + g(y_n^{i+1}) + g(y_n^{i-1}) - 2g(y_n^i) \tag{6}$$

preserves the quantity $\sum_i y_n^i$.

3. LYAPUNOV ANALYSIS OF SPATIOTEMPORAL CHAOS

Lyapunov exponents are the main statistical tool for the study of low-dimensional strange attractors, since they measure the linear instability of trajectories in phase space. Moreover they can be related to other ergodic indicators such as entropies and dimensions.[1] In extended systems, whenever many interacting modes are present, both temporal and spatial instabilities must be taken into account. Two complementary approaches have been developed which are based, respectively, on the temporal

(spatial) growth rate of space (time) periodic perturbations. The former approach is the standard method to determine the spectrum of Lyapunov exponents. The latter one, which leads to the introduction of spatial exponents, is useful both in revealing the localization properties of Lyapunov vectors[4] and characterizing the stability of open-flow systems.[14]

Numerical simulations[15] and approximate analytical results[16] indicate that a well-defined thermodynamic limit for the set of Lyapunov exponents is reached for large enough system size, both in space and time. As a consequence, the Kaplan–Yorke dimension and the Kolmogorov–Sinai entropy are extensive quantities,[17] so that the dynamics of a long chain can be roughly seen as that of many independent adjacent subchains. This fact allows us to define Lyapunov spectra independent of the system size (see below).

The following two subsections are dedicated to a brief review of the above-mentioned definitions. For simplicity we limit ourselves to the symmetric CML case, Eq. (3); the extension to spatiotemporal flows is straightforward.

3.1. Temporal Lyapunov Exponents

The standard Lyapunov spectrum is obtained by following the evolution of a perturbation δy_n^i in the tangent space with periodic boundary conditions assumed for it. A more general class of Lyapunov exponents has been introduced in ref. 3 by enlarging the set of allowed perturbations to include exponentially shaped profiles such as $\delta y_n^i = \Phi_n^i e^{\mu i}$. The evolution equation for the scaled variable Φ_n^i reads

$$\Phi_{n+1}^i = m_n^i \left[\frac{\varepsilon}{2} e^{-\mu} \Phi_n^{i-1} + (1-\varepsilon)\, \Phi_n^i + \frac{\varepsilon}{2} e^{\mu} \Phi_n^{i+1} \right] \tag{7}$$

where

$$m_n^i = f' \left(\frac{\varepsilon}{2} y_n^{i-1} + (1-\varepsilon)\, y_n^i + \frac{\varepsilon}{2} y_n^{i+1} \right)$$

is the local multiplier, and Φ_n^i obeys periodic boundary conditions. The exponents $\lambda_j(\mu)(1 \leqslant j \leqslant L)$ obtained from the iteration of Eq. (7) for a fixed value of μ will be hereafter called *temporal* Lyapunov exponents (called "specific" exponents in ref. 3). The resulting temporal Lyapunov spectrum (TLS) is defined in the limit $L \to \infty$ as

$$\lambda(\mu, n_\lambda) = \lambda_j(\mu), \qquad n_\lambda = j/L \tag{8}$$

where the integrated density (the fraction of exponents smaller than λ) n_λ ranges, by construction, between 0 and 1. For $\mu = 0$ the standard TLS is recovered. Exactly the same arguments apply to continuous-time models such as, e.g., chains of coupled oscillators. When the space, too, is continuous, the only difference is that n_λ is unbounded from above.

It is well known that the computation of Lyapunov exponents from Eq. (7) proceeds through the construction of an ordered sequence of Lyapunov vectors (i.e., an orthonormal basis), which generate the most expanding subspaces of increasing dimension.[18] In general, the direction of such vectors depends on the point in phase space where they are computed. These fluctuations make an analytic treatment of the linear stability problem hardly feasible. However, their spatial structure can be clarified by following in space the evolution of perturbations. This is precisely the subject of the next section.

3.2. Spatial Lyapunov Exponents

Spatial Lyapunov exponents have been introduced as a tool for investigating the structure of temporal Lyapunov vectors.[4] By assuming a temporal exponential profile for the perturbation, $\delta y_n^i = e^{\lambda n} \Psi_n^i$, we have that the evolution equation in tangent space reads

$$\Psi_{n+1}^i = e^{-\lambda} m_n^i \left[\frac{\varepsilon}{2} \Psi_n^{i-1} + (1-\varepsilon)\, \Psi_n^i + \frac{\varepsilon}{2} \Psi_n^{i+1} \right] \tag{9}$$

which, in turn, can be seen as a spatial recursive equation,

$$\begin{aligned} \Theta_n^{i+1} &= \Psi_n^i \\ \Psi_n^{i+1} &= -2 \frac{1-\varepsilon}{\varepsilon} \Psi_n^i + \frac{2e^\lambda}{\varepsilon m_n^i} \Psi_{n+1}^i - \Theta_n^i \end{aligned} \tag{10}$$

with boundary conditions $\Theta_{T+1}^i = \Theta_1^i$, $\Psi_{T+1}^i = \Psi_1^i$. Equations (10) provide the starting point of a transfer matrix approach. In fact, by introducing the column vector $\mathbf{v}(i) \equiv (\Theta_1^i, \Theta_2^i, \ldots, \Theta_T^i, \Psi_1^i, \ldots, \Psi_T^i)'$, we can describe the spatial evolution in terms of products of matrices of the form

$$J^i = \begin{pmatrix} 0 & 1 \\ -1 & A^i \end{pmatrix} \tag{11}$$

where 0 and 1 are the $(T \times T)$ null and identity matrix, and A^i is a bidiagonal matrix, with $A_{n,n}^i \equiv -2(1-\varepsilon)/\varepsilon$ and $A_{n,n+1}^i \equiv 2e^\lambda/(\varepsilon m_n^i)$. Since

det $J^i = 1$, the spatial dynamics is "conservative." Numerical implementation of this method requires the knowledge of the local multipliers m_n^i, which have to be computed, in principle, for a generic orbit of period T. In practice, it is assumed that boundary conditions are irrelevant in the thermodynamic limit $T \to \infty$, and that any initial condition chosen according to the invariant measure is almost equivalent.

For a given T, there exist $2T$ Lyapunov exponents μ_j. This doubling in the number of the degrees of freedom is related to the two-step spatial memory of Eqs. (10). Moreover, since $J^i = (J^i)^{-1}$, the spatial Lyapunov spectrum (SLS) associated with any symmetric trajectory is invariant under "space" reversal $i \to -i$, i.e., $\mu_j = -\mu_{T+1-j}$. Notice that this is no longer true for models like (4) with a $\alpha \neq 1/2$. In analogy to the TLS, the SLS is defined in the limit $T \to \infty$ as

$$\mu(\lambda, n_\mu) = \mu_j(\lambda), \qquad n_\mu = \frac{j - 1/2}{T} - 1 \tag{12}$$

where j denotes the jth spatial Lyapunov exponent. The term $1/2T$ is a finite-size correction, introduced to fix the center of symmetry at $n_\mu = 0$, independently of the size T. The density n_μ of spatial exponents ranges between -1 and 1.

In analogy with disordered systems, the minimum positive exponent $\mu(\lambda, 0)$ can be interpreted as the inverse of the localization length l of the Lyapunov vector, provided that λ belongs to the TLS.

The direct implementation of the above method faces the difficulty that iteration of the nonlinear equation in space usually does not converge onto the same attractor as obtained by iterating in time the original model. In fact, it turns out that the invariant spatiotemporal measure corresponds to a strange repeller in space (this point will be elucidated in the second part). Thus, one must first generate a 2D pattern of local multipliers and then use it in the computation of the spatial Lyapunov exponents.

4. THE (μ, λ) SPACE

A more symmetric representation of both spatial and temporal spectra is obtained by expressing Eqs. (8) and (12) as $n_\lambda(\mu, \lambda)$ and $n_\mu(\mu, \lambda)$. Both functions are well defined insofar as λ and μ are monotonously decreasing for increasing density. Any point (μ, λ) identifies a specific perturbation growing as $e^{\lambda n}$ in time and as $e^{\mu i}$ in space. The integrated density $n_\mu(n_\lambda)$ corresponds to the normalized number of "modes" with spatial (temporal) exponent smaller than $\mu(\lambda)$.

The set $\mathscr{D}$ of points in the (μ, λ) plane corresponding to admissible perturbations is identified by simultaneously requiring.

$$\frac{\partial n_\mu}{\partial \mu} \geqslant 0, \qquad \frac{\partial n_\lambda}{\partial \lambda} \geqslant 0 \tag{13}$$

One should notice a similarity with the dispersion relation for wave propagation: given a specific spatial profile, the temporal growth rate is bounded in a given interval from the above inequalities. The boundaries $\partial\mathscr{D}_\mu$ and $\partial\mathscr{D}_\lambda$ of the domain $\mathscr{D}$ are obtained by setting the l.h.s. equal to zero in Eq. (13). In Fig. 1 we report such borders for a chain of coupled logistic maps $[f(x) = 4x(1-x)]$ and (a) $\varepsilon = 1/3$ and (b) $\varepsilon = 2/3$. As the two borders coincide in both cases, we have a first indication that n_μ and n_λ are not independent of one another: this is not surprising, since both quantities arise from the iteration of the same set of linear equations. The invariance of the dynamical equations under the transformation $i \to -i$ implies a left-right symmetry of the border $\partial\mathscr{D}$ (we drop the subscript whenever $\partial\mathscr{D}_\mu = \partial\mathscr{D}_\lambda$). The upper and lower boundaries at $\mu = 0$ correspond to the standard maximum $\lambda_{\max}$ and minimum $\lambda_{\min}$ Lyapunov exponents (for $\varepsilon = 2/3$, $\lambda_{\min} = -\infty$[9]). Three typical representatives of temporal and spatial spectra are reported in Fig. 2a–2c and 2d–2f, respectively, with reference to $\varepsilon = 1/3$. The SLS obtained for $\lambda_{\min} \leqslant \lambda \leqslant \lambda_{\max}$ is characterized by a single band, while for larger and smaller values of λ two symmetric bands appear. The TLS appears to be characterized by a single band for any value of μ. For $\varepsilon = 1/3$ the size of the band increases monotonously up to $\mu = \mu_c$, where the minimum exponent diverges to $-\infty$, while in the latter case the divergence occurs at $\mu = 0$. Above μ_c, the size of the band shrinks to zero and its position increases linearly with μ.

This can be easily understood by realizing that, for large μ, Eq. (7) reads

$$\Phi_{n+1}^i \approx m_n^i \frac{\varepsilon}{2} e^\mu \Phi_n^{i+1} \tag{14}$$

Accordingly, the asymptotic value of the Lyapunov exponent is

$$\lambda \approx \mu + \log(\varepsilon/2) + \langle \log |m_n^i| \rangle \tag{15}$$

where the average $\langle \cdot \rangle$ should be taken along the line $i = l - n$ for any given l. Equation (15) is increasingly accurate for $\mu \to \infty$, when the evolutions along the lines $i = l - n$ are exactly decoupled, so that an infinite degeneracy in the spectrum is necessarily found. It is transparent from

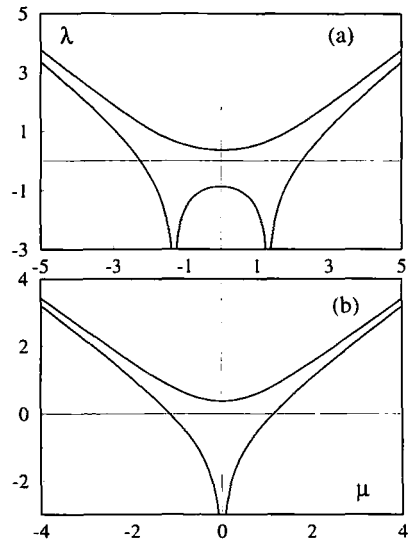

Fig. 1. Plot of the boundary $\partial\mathscr{D}$ for the logistic CML for two values of the coupling: (a) $\varepsilon = 1/3$, (b) $\varepsilon = 2/3$.

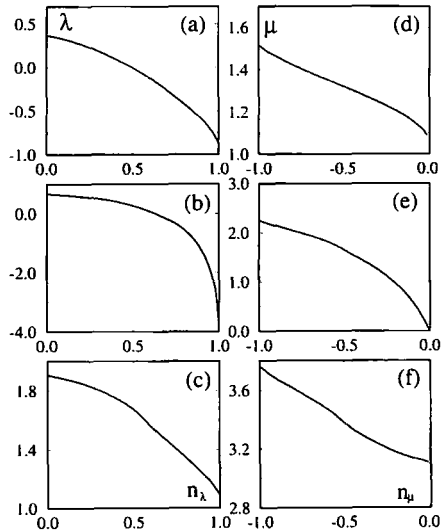

Fig. 2. Temporal Lyapunov spectra for the logistic CML ($\varepsilon = 1/3$) for (a) $\mu = 0$, (b) $\mu = 1.31$ (i.e., μ_c), and (c) $\mu = 3.0$; and Spatial Lyapunov spectra for the same diffusive coupling and (a) $\lambda = -2.0$, (b) $\lambda = 0$, and (c) $\lambda = 2.0$.

Eq. (15) that the slope of the branch must be equal to 1. Such a value is nothing but the limit velocity for the propagation of disturbances in a lattice with nearest neighbor interactions. In fact, in the case of a coupling extended to s neighbors, Eq. (14) becomes $\Phi^i_{n+1} \approx m^i_n \varepsilon e^{s\mu} \Phi^{i+s}_n / 2$, so that the slope is, in general, equal to the number of neighbors s. Finally, notice that $\log(\mu/2) + \langle \log |m^i_n| \rangle$ indicates the intersection of the asymptote with the vertical axis.

The above phenomenology turns out to be rather general: simulations performed with several different maps exhibit the same behavior as long as one limits the analysis to nearest neighbor coupling.

In the literature, the standard TLS is generally reported using n_λ as the independent variable. This representation offers a natural interpretation of the Kaplan–Yorke conjecture[17] and it can be extended to our more general framework with two independent variables. In fact, it turns out that any pair (n_μ, n_λ) identifies unambiguously a spatiotemporal perturbation, exactly in the same way as μ and λ do. The two integrated densities are, by construction, normalized in the rectangle $[-1, +1] \times [0, +1]$. Numerical simulations performed on logistic maps show that the domain $\mathscr{D}$ in the (μ, λ) plane corresponds to a domain $\mathscr{B}$ which, strangely enough, does not coincide with the full rectangle, and indeed only points with $n_\lambda > |n_\mu|$ are obtained (see Fig. 3). We have no explanation for this phenomenon.

The four lines identifying the border $\partial\mathscr{D}$ are mapped onto the four distinct points $P = (0, 0)$, $Q = (0, 1)$, $R_+ = (1, 1)$, and $R_- = (-1, 1)$. A detailed characterization of the mapping in presented in Fig. 3. Symmetry reasons

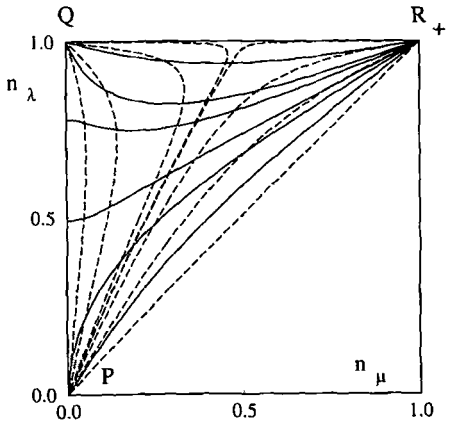

Fig. 3. Schematic plot of lines with constant λ (solid lines) and μ (dashed lines) and the boundary $\partial\mathscr{B}$ of the allowed region in the (n_μ, n_λ) plane.

require that the line $\mu = 0$ is mapped onto the line $n_\mu = 0$. All vertical lines in the (μ, λ) plane correspond to curves departing from P in (n_μ, n_λ). Their ending point E depends on μ: for $\mu < -\mu_c$, $E = R_+$; for $-\mu_c < \mu < \mu_c$, $E = Q$; and for $\mu > \mu_c$, $E = R_-$. The critical curves for $\mu = \pm\mu_c$ are straight lines arriving at $(\pm 0.5, +1)$.

The images of all the horizontal lines connect R_- with R_+ exhibiting an obvious symmetry with respect to n_μ. All curves corresponding to $\lambda < \lambda_{\min}$ pass through the point Q. Analogously, those with $\lambda > \lambda_{\max}$ pass through P.

We can thus conclude by remarking that there is a sort of duality between the two representations. In fact, the four segments delimiting $\mathscr{B}$ correspond to four points in the (μ, λ) plane, more precisely to $(\pm\infty, +\infty)$ and $(\pm\mu_c, -\infty)$ in Fig. 1.

In order to examine the generality of the above scenario in the following subsections we discuss two specific cases: (a) a spatially homogeneous and stationary pattern, which can be analytically treated, and (b) spatiotemporal periodic orbits.

4.1. Homogeneous Chains

The simplest chaotic dynamics one can think of is the evolution of piecewise linear maps of the type $f(x) = rx \pmod 1$. In this case, the local multiplier is everywhere constant (both in space and time). The resulting Lyapunov spectra coincide with those of spatiotemporal fixed points (stationary and homogeneous solutions). The TLS is easily obtained by noticing that the associated eigenvectors are nothing but the Fourier modes e^{iqj} (where j is the imaginary unit) of the chain. The TLS can be determined by Fourier transforming Eq. (7), which allows calculating the multiplier m for a given wavenumber q. The Lyapunov exponent $\lambda(\mu, n_\lambda) = \log|m|$ is

$$\lambda(\mu, n_\lambda) = \log r + \tfrac{1}{2}\log|(1-\varepsilon)^2 + 2\varepsilon(1-\varepsilon)\cosh\mu\cos\pi n_\lambda + \varepsilon^2(\cosh^2\mu - \sin^2\pi n_\lambda)| \tag{16}$$

where n_λ is equal to the spectral density q/π, since, by virtue of the node theorem, all the multipliers are naturally ordered with q.

The same technique can be used to evaluate the SLS, the only difference being the twostep spatial memory in Eqs. (10). The spectral problem can be solved by determining the eigenvalues of suitable 2×2 matrices, obtaining

$$\mu(\lambda, n_\mu) = \frac{1}{2}\cosh^{-1}\left[\frac{a + [(a-\varepsilon^2)^2 + \varepsilon^2 e^{2\lambda}\sin^2(\pi n_\mu)]^{1/2}}{\varepsilon^2}\right] \tag{17}$$

where

$$a=\frac{r^2(1-\varepsilon)^2-2r(1-\varepsilon)\cos\pi n_\mu e^{2\lambda}}{2} \tag{18}$$

Equations (16) and (17) can be inverted to give the integrated densities

$$n_\lambda^{\pm}=\frac{1}{\pi}\arccos\left[\frac{-r(1-\varepsilon)\cosh\mu\pm[r^2(1-2\varepsilon)\sinh^2\mu+e^{2\lambda}]^{1/2}}{\varepsilon r}\right] \tag{19}$$

$$n_\mu^{\pm}=\frac{1}{\pi}\arccos\left[\frac{-r(1-\varepsilon)\sinh^2\mu\pm\cosh\mu[r^2(1-2\varepsilon)\sinh^2\mu+e^{2\lambda}]^{1/2}}{e^{\lambda}}\right] \tag{20}$$

For $\varepsilon<1/2$, only the positive solution exists, so that $n_\lambda=n_\lambda^+$ and $n_\mu=n_\mu^+$. For $\varepsilon>1/2$ both solutions are acceptable. In fact, the spectrum of multipliers m passes through zero and then $n(\log|m|)$ is no longer invertible. In this case, two branches exist, ordered in an opposite way with respect to λ. The integrated density of Lyapunov exponents is obtained by summing the contributions arising from the two partly overlapping bands,

$$n_\lambda=n_\lambda^+ +(1-n_\lambda^-)$$

and

$$n_\mu=\begin{cases}n_\mu^+-n_\mu^- & \text{for} \quad -1\leqslant n_\mu^{\pm}\leqslant 0\\ n_\mu^+ +(1-n_\mu^-) & \text{for} \quad 0\leqslant n_\mu^{\pm}\leqslant 1\end{cases}$$

The analytic expressions of the border $\partial\mathscr{D}$ can be explicitly obtained by imposing that the argument of the arccosine function in n_λ is ± 1. For $\varepsilon<1/2$ this procedure yields

$$\lambda=\log r+\log|\varepsilon\cosh\mu\pm(1-\varepsilon)| \tag{21}$$

For $\varepsilon>1/2$, the upper border is unchanged (plus sign), while the lower one is now obtained from the identification of the inversion point where $n_\lambda^+=n_\lambda^-$,

$$\lambda=\log r+\log|(2\varepsilon-1)^{1/2}\sinh\mu| \tag{22}$$

It should be noticed that the expressions of the borders as obtained from Eq. (19) or Eq. (20) are identical. The two borders reported in Fig. 1 for logistic maps are qualitatively the same as those obtained in the present case for $\varepsilon<1/2$ and $\varepsilon>1/2$, respectively.

Moreover, from Eqs. (21) and (22)

$$\mu_c = \begin{cases} \pm \cosh^{-1}\left(\dfrac{1-\varepsilon}{\varepsilon}\right) & \text{if} \quad \varepsilon \leqslant 1/2 \\ 0 & \text{otherwise} \end{cases}$$

The value of μ_c is independent of the map f. In fact, the Jacobian matrix can be factorized as the product of two matrices, the former containing the detail of the local dynamics, the latter being the diffusion operator, which depends only on μ and ε. It turns out that it is precisely the determinant of the latter operator which vanishes at $\mu = \mu_c(\varepsilon)$. This singular behavior is associated with the existence of a Fourier mode, $(-1)^i$, which is killed in just one iterate.

Extension of the above analysis to asymmetric CML (4) yields the following expressions for the borders;

$$\lambda = \log r + \log |\varepsilon e^{-\mu} + 2\alpha \sinh \mu \pm (1-\varepsilon)| \tag{23}$$

$$\lambda = \log r + \log \left| \left(\varepsilon^2 - \frac{(1-\varepsilon)^2}{4\alpha(1-\alpha)} \right)^{1/2} (\alpha e^{\mu} - (1-\alpha)\, e^{-\mu}) \right| \tag{24}$$

which generalize Eqs. (21) and (22), respectively. Two examples of boundaries are reported in Fig. 4 for $\alpha = 3/4$ and $\alpha = 1$. The curves are still symmetric, though now the center of symmetry is $\tilde{\mu} = \log[(1-\alpha)/\alpha]/2$. For decreasing (increasing) values of α from 1/2, the left singularity moves toward $-\infty(+\infty)$ and eventually disappears at $\alpha = 0(1)$.

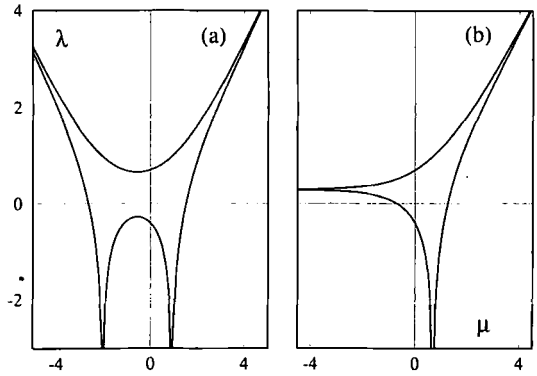

Fig. 4. Plot of the boundary $\partial\mathscr{D}$ for the asymmetric homogeneous chain for $\varepsilon = 1/3$: (a) $\alpha = 3/4$, (b) $\alpha = 1$.

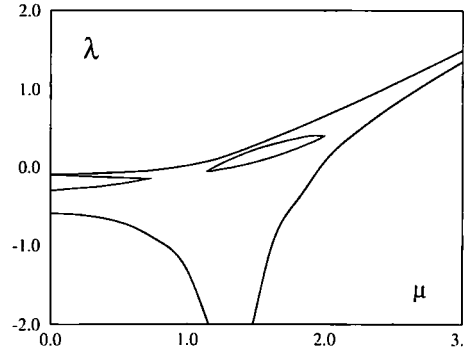

Fig. 5. Plot of the boundary $\partial\mathscr{D}$ for a spatiotemporal periodic orbit (period 3 in space and 2 in time).

Finally, one should notice that all the results contained in this subsection apply also to the case of a homogeneous random evolution: the only difference is that $\log r$ is to be everywhere replaced with the average value $\langle \log |m_n| \rangle$.

4.2. Periodic Orbits

An interesting representation of the stability properties in the (μ, λ) plane is obtained for periodic (both in space and time) orbits. It was already noticed in ref. 3 that the standard TLS exhibits a band structure. This feature generalizes to the presence of a series of holes within the domain $\mathscr{D}$. The structure of the temporal spectra is determined from the spatial periodicity and vice versa. More precisely, the number of bands of the TLS (SLS) can be at most equal to the spatial period (twice the temporal period). The borders $\partial\mathscr{D}$ are reported in Fig. 5 for a hypothetical orbit of period 3 in space and 2 in time. Since the reference to a specific CML model is not of particular relevance in this case, the values of the six multipliers have been chosen *a priori* without any relation to a preassigned dynamics. As the integrated densities remain constant inside each hole, the latter are mapped onto single points in the (n_λ, n_μ) plane which are analogous to P, Q, and $R_\pm$.

5. LOCALIZATION IN TANGENT SPACE

The localization of Lyapunov vectors observed in refs. 4, 19 and 20 implies that a generic perturbation is sensibly amplified in a limited spatial region. Heuristically this phenomenon can be explained by noticing the

analogy with the Anderson localization problem. The presence of the discrete Laplacian operator makes Eq. (7) similar to a wave equation on a lattice, or to a Schrödinger equation in the tight-binding approximation. Chaotic fluctuations of the multipliers play the same role as a time-dependent disorder in the above problems.

A further analogy exists between the spatial evolution and the stationary 2D Anderson model, defined by the equation

$$\psi_n^{i-1} + \psi_n^{i+1} + \psi_{n-1}^i + \psi_{n+1}^i = (\omega - V_n^i)\,\psi_n^i \tag{25}$$

where ω is the rescaled energy of the eigenstate ψ_n^i and V_n^i is the random potential bounded between $-W/2$ and $W/2$. In this case, both ω and W can be interpreted as control parameters in a dynamical equation. The main difference from Eqs. (10) is that now also the index n denotes a spatial direction. The lack of time-reversal invariance in the CML is reflected in the absence of a term proportional to Ψ_{n-1}^i.

On the basis of this simple analogy, one might expect that spatially chaotic solutions of Eqs. (10), characterized by pseudo-random sequences of multipliers m_n^i, are associated with localized vectors. In fact, the theoretical analysis of the 2D Anderson model predicts the existence of exponentially localized eigenfunctions for arbitrarily weak disorder.[21] On the other hand, numerical simulations[4] show that $\mu(\lambda, 0)$ is always 0 for λ belonging to the standard TLS, implying that the localization is not purely exponential. This contradiction can be resolved by noticing that in the CML case, at variance with the Schrödinger problem, the transfer matrices are iterated assuming an exponential profile along the transverse direction. Accordingly, different operators are involved in the two procedures, with an evident symmetry breaking in the latter case.

Since $\mu(\lambda, 0)$ yields the localization length l, it is reasonable to speculate that, whenever $\mu(\lambda, 0) = 0$, the behavior of the SLS in the vicinity of $n_\mu = 0$ gives information about a supposedly lower-than-exponential decay of the Lyapunov vector. A first necessary condition for this conjecture to be true is that the convergence (for $T \to \infty$) of the SLS to its asymptotic shape is sufficiently fast so as to guarantee that the finite-size value of the minimum positive exponent is essentially determined by the difference of the corresponding n_μ from 0, i.e.,

$$\mu_T(\lambda) \approx \mu\left(\lambda, -\frac{1}{2T}\right) \tag{26}$$

This point will be discussed in the last subsection of this section; here we limit ourselves to noting that numerical simulations reveal that the convergence is not always sufficiently fast.

Assuming a power-law behavior of the SLS, i.e.,

$$\mu \sim |n_\mu|^\gamma, \qquad n_\mu \to 0 \tag{27}$$

and Eq. (26) to hold, then the vector δy_n^i decays as $\exp[-L/l(T)] \sim \exp[-L/T^\gamma]$. Whenever there is a perfect symmetry between spatial and temporal directions, as in the Anderson model (25), T can be replaced by L in the above expression, yielding a decay behavior

$$\delta y_n^L \sim \exp[-L^{(1-\gamma)}] \tag{28}$$

Accordingly, if $0 < \gamma < 1$, a stretched-exponential envelope is obtained. We should anyhow recall that T and L are not in general interchangeable, so that the above picture is only approximately correct.

5.1. Frozen Random Patterns

For stationary but spatially chaotic states, the evolution in tangent space is mapped exactly onto a 1D localization problem. In this case, it is rigorously proved that all the eigenvectors are exponentially localized. Thus, qualitative differences from the scenario depicted in the previous section are expected. Indeed, frozen random patterns are, to our knowledge, the only case where the borders derived from spatial and temporal spectra do not match. This is illustrated in Fig. 6, where it is clearly seen that the spatial Lyapunov exponents[4] are all bounded away from zero. As a consequence there is a pair of borders which cannot be revealed by the temporal analysis (see dashed line in Fig. 6). In fact, upon increasing μ from 0, both the maximum and minimum temporal Lyapunov exponents are constant until the spatial border is reached (for clarity, only the behavior of the maximum exponent is reported in Fig. 6). At larger values of μ, the two borders coincide.

The anomalous structure of $\mathscr{D}$ is a consequence of the exponential localization of the temporal Lyapunov vectors. In fact, the dashed curve is nothing but $1/l$ for all temporal exponents belonging to the spectrum.

A further interesting feature concerns the identification of the critical value μ_l where the upper temporal border departs from the spatial one. By noticing that the upper border is the Legendre transform[3] of the maximal comoving Lyapunov exponent,[5] it appears natural to conjecture that $\partial\mathscr{D}_\lambda$ can be obtained from $\partial\mathscr{D}_\mu$ by means of a standard construction to remove

[4] Temporal homogeneity allows reducing the transfer matrix approach to a product of 2×2 matrices.

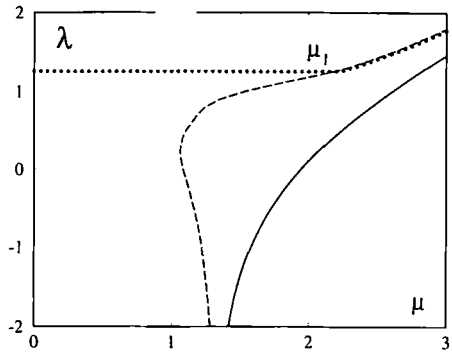

Fig. 6. Plot of the boundary $\partial\mathscr{D}$ for a frozen random pattern. Dots and lines refer to temporal and spatial exponents respectively. Below $\mu = \mu_l$, $\partial\mathscr{D}_\lambda \neq \partial\mathscr{D}_\mu$.

all changes of concavity. In other words, we expect μ_l to be located at the inflection point of $\partial\mathscr{D}_\mu$. This seems indeed to be true. We shall comment more extensively about this point in the second part of the paper.

5.2. Symplectic Maps

There is a strict analogy between the application of the transfer matrix approach to the Anderson model (25) and the computation of Lyapunov spectra in Hamiltonian systems, since in both cases one deals with products of "random" symplectic matrices.[19] Generally speaking, both the symplectic structure and the time-reversal invariance induce a "pairing" in the Lyapunov spectrum which turns out to be invariant under the transformation $\lambda \to -\lambda$. Consequently, a similar structure of the borders is expected along the μ and λ directions. Obviously, in the Anderson model both are spatial directions and they can be exactly interchanged, so that we expect the exact invariance under the transformation $(\mu, \lambda) \to (\lambda, \mu)$.

The main difference with respect to the previous class of dissipative CML is the slope of the lower asymptotes, which are now tilted at a $\pm\pi/4$ angle. This is precisely the consequence of the invertibility of mapping (5). Indeed, when the evolution is reversed in time, the maximum velocity of propagation of a disturbance is 1 (when nearest neighbor coupling is assumed). This fact allows us to interpret the vertical asymptotes in Fig. 1 as an indication of an infinite (backward) velocity. The noninvertibility of the dynamics leads to a global unavoidable ambiguity of the preimage already in one step.

Simulations of model (5) show two qualitatively different domain structures. Indeed, depending on the nonlinearity k, a hole may exist

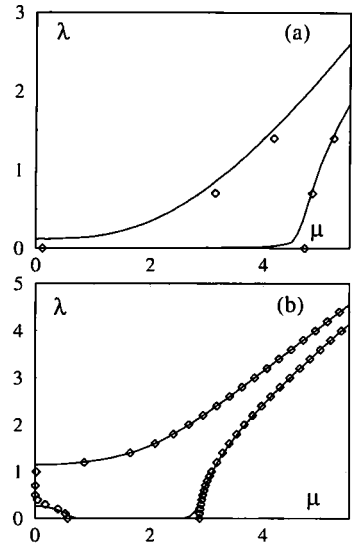

Fig. 7. Plot of the boundary $\partial\mathscr{D}$ for coupled standard maps (a) $k = 0.5$, (b) $k = 4.0$. Symbols refer to spatial exponents, while the lines are obtained from the temporal spectrum.

around $(\lambda, \mu) = (0, 0)$, indicating that the standard TLS is made of two distinct bands. The two possibilities are illustrated in Fig. 7, where $\partial\mathscr{D}$ is reported for $k = 0.5$ and $k = 4.0$. At variance with the latter case, at $k = 0.5$ a substantial disagreement is found between spatial and temporal borders. This artifact seems to be caused by strong finite-size effects in the convergence of the SLS to its asymptotic form. This may be connected with the slowly decaying temporal correlations (up to time of order 10^3) previously revealed by the analysis of diffusion properties[22] and of effective Lyapunov exponents[12].

To close this section, we want to remark that the theory developed in ref. 21 the 2D Anderson problem, predicting that all states are exponentially localized, would imply the presence of a hole at $(\lambda, \mu) = (0, 0)$ for any value of k in the present case. On the other hand, direct numerical simulations of model (25) appear to be quite inconclusive due to the rapid divergence of the localization length for $W \to 0$.[23] Thus, also in our dynamical model it is not possible to conclude whether there are two truly distinct regimes as suggested by Fig. 7.

5.3. Localization and Spatiotemporal Chaos

In this subsection we turn again to the general case of spatiotemporal chaos, reporting some results on the power-law singularity in the SLS. In

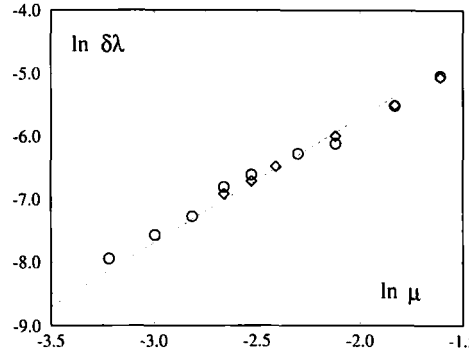

Fig. 8. Scaling of the maximum temporal exponent around $\mu = 0$; logistic maps with random (circles) or deterministic (diamonds) dynamics, $\varepsilon = 1/3$. The dashed line has slope 2.

general, for λ belonging to the standard TLS, the corresponding SLS exhibits a linear behavior around $n_\mu = 0$, that is, $\gamma = 1$ [see Eq. (27)]. Hence, according to Eq. (28), the Lyapunov vector decays more slowly than a stretched exponential. In fact, direct numerical investigations reveal a power-law localization.[24]

The only exception to the above picture is represented by the extrema of the standard spectrum, i.e., $\lambda = \lambda_{\min}, \lambda_{\max}$, where γ values substantially smaller than 1 are observed. This is not surprising, in that these are the points where a gap is closing in the SLS (see, for example, Fig. 1). Although this singularity arises at a band merging point in the (μ, λ) plane, γ is not trivially linked with the shape of the boundary around $\mu = 0$. In fact, while γ may depend on the model, the shape of $\partial\mathscr{D}$ around $\mu = 0$ turns out to be always parabolic. This has been verified both analytically for homogeneous chains by expanding Eq. (17) around $\mu = 0$, and numerically for various models [see Fig. 8, where $\delta\lambda = \lambda(\mu, 0) - \lambda_{\min}$ is plotted versus μ].

Extensive numerical simulations have been performed on several classes of CMLs to measure γ, namely model (3) with logistic, tent, skewed, and Bernoulli maps, the model with linear coupling (2), and symplectic maps (5) (see Fig. 9). The mapping functions as well as the measured values of a are reported in Table I, indicating that the exponent is either approximately equal to 1/3 or to 1/2. The inaccuracy is essentially to be attributed to finite-size effects, as the maximum temporal exponent has been always computed with a relative error of 10^{-3}. Actually, the above estimates can be improved by assuming that the spectrum is an analytic function of n_μ^γ. More precisely, the power-series expansion of μ to the second order,

$$\mu \approx a n_\mu^\gamma + b n_\mu^{2\gamma} \tag{29}$$

Table I. Singularity Exponent γ of the SLS for CML Models, Eq. (3), with Various Mapping Functions $f(x)$ of the Interval [0, 1][a]

CML model	γ
Tent	0.37
Tent (rnd)	0.36
Logistic	0.32
Logistic (rnd)	0.32
Linearly coupled	0.32
Symplectic	0.31
Skewed Bernoulli	0.54
Skewed Bernoulli (rnd)	0.45
Cubic	0.49

[a] $f(x) = 1 - |2x - 1|$ (tent), $f(x) = 4x(1-x)$ (logistic), $f(x) = 3x$ for $x < 1/3$ and $f(x) = (3x-1)/2$ otherwise (skewed Bernoulli), $f(x) = 3/2x + x - x^3 \pmod 1$ (cubic). Linearly coupled maps refer to Eq. (2) with $F(x) = 4x/(x^4+1)$ and symplectic to Eq. (5) with $k = 4.0$. In every case a coupling $\varepsilon = 1/3$ is taken. The label rnd refers to random multipliers with the same distribution as that of the corresponding CML.

can be used to fit the numerical data in the vicinity of $\mu = 0$, in order to determine the parameters a and b for a given γ. The best estimate of the exponent γ is finally determined as the one which optimizes the fit. As a result of this application the γ values are even closer to 1/3 and 1/2, confirming that there are two universality classes. The analysis of the considered models reveals that the exponent 1/2 is obtained only when the local variable is scalar and if the local multipliers are all positive (negative). Hence the exponent 1/3 seems to arise from "dephasing" effects due to a local rotation of the perturbation (if the variable is a vector) or to the randomness of the sign of the multipliers (if the variable is a scalar). The larger generality of the latter value is further confirmed by its observation in very different contexts such a band random matrices[25] or nonequilibrium molecular dynamics.[26]

A further interesting interpretation of the two universality classes appears from the structure of the temporal evolution in tangent space [Eq. (7)]. Pikovsky and Kurths[27] have shown that the equation resulting from the change of variable $h_n^i = \ln \delta y_n^i$ is approximately equal to a discrete

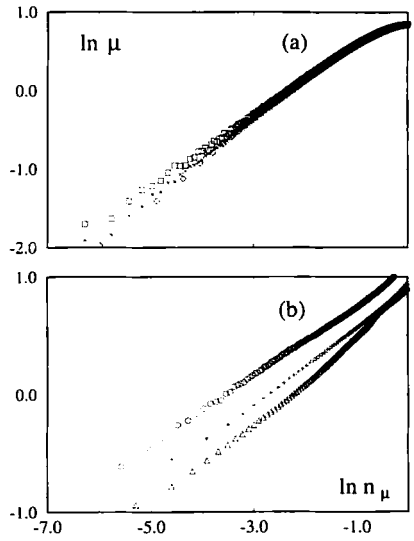

Fig. 9. Singularity of the spatial spectra ($\varepsilon = 1/3$): (a) skewed piecewise CML with deterministic (diamonds) and random (crosses) multipliers, and cubic CML (squares) (1/2 singularity); (b) logistic CML with deterministic (triangles) and random (plus) multipliers, and symplectic CML (circles) (1/3 singularity). Details on the mapping functions and the bestfit values of the exponents are reported in Table I.

version of the Kardar–Parisi–Zhang equation[28] for the scalar field $h(x, t)$ (x and t replace i, and n, respectively)

$$\partial_t h = \eta_1 \partial_x^2 h + \eta_2 (\partial_x h)^2 + \xi \tag{30}$$

where $\xi(x, t) = \ln m_n^i$ is a noise term arising from space-time chaos, and $\eta_{1,2}$ are two constants. A first limitation to an exact correspondence stems from higher order spatial derivatives the presence of which should not affect the scaling behavior.[28] A more relevant difference arises when the sign of m_n^i is a fluctuating quantity, since the definition itself of h_n^i is meaningless, as already argued in ref. 27. According to our previous considerations, γ turns out to be 1/2 if and only if the reduction to Eq. (30) is possible. In such cases, from Eq. (28), we expect for the Lyapunov vector a stretched exponential profile $\delta y_n^L \sim \exp(-L^{1/2})$, which is perfectly consistent with the prediction that the field h describes a Brownian motion in space. Thus, the presence of the exponent $\gamma = 1/3$ seems to call for a different stochastic model.

Finally, let us recall that the exponent γ can provide information about the localization of δy_n^i only when the convergence of the SLS is

sufficiently fast. For instance, the exponent $\gamma = 1/2$ is observed also for a homogeneous chain, where no localization is obviously present. The apparent contradiction is solved by noticing that in this case the Tth spatial exponent is exactly equal to 0 for any T. Therefore, γ does not describe the convergence of the minimum positive exponent as expected, and the above arguments are no longer valid.

5.4. Singularities in the TLS

For the sake of completeness, we briefly discuss also an example of a singularity occurring in the TLS, which is not related to localization features of Lyapunov vectors, but rather to the existence of a conserved parameter.

All singularities in SLS discussed in the previous section are characterized by $\gamma < 1$, that is, by a vanishing density of Lyapunov exponents. The study of TLS in models with a conserved quantity, such as Eq. (6), has revealed the existence of the complementary phenomenon, too, i.e., a power-law divergence in the density of exponents

$$\frac{dn_\lambda}{d\lambda} \sim \frac{1}{|\lambda|^\beta} \tag{31}$$

around $\lambda = 0$.[29] By calling n_c the integrated density determined by the condition $\lambda(0, n_c) = 0$, the above equation can be rephrased as $|\lambda| \sim |n_\lambda - n_c|^\nu$ with $\nu = 1/(1-\beta)$. Figure 10 shows the scaling behavior around the critical integrated density n_c for model (6) with $g(x) = \varepsilon_1 \sin(2\pi x) + \varepsilon_2 x$ ($\varepsilon_{1,2}$ are

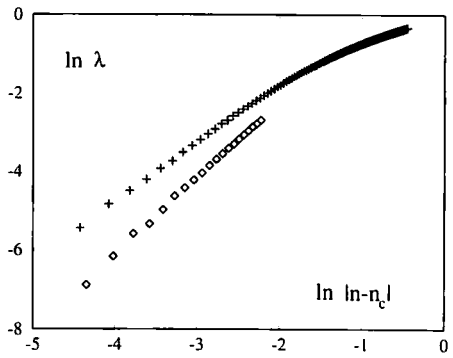

Fig. 10. Singularity of the temporal spectra of CML (6) with conserved quantity: $g(x) = \varepsilon_1 \sin(2\pi x) + \varepsilon_2 x$, $\varepsilon_1 = 1/5$, and $\varepsilon_2 = 1/20$. The critical value of the integrated density is $n_c = 0.643$.

two coupling constants). Crosses and diamonds correspond to approaching $\lambda = 0$ from above and below, respectively. The different slopes (ν about 1.5 in the former case and 2 in the latter) confirm the existence of two distinct critical behaviors as conjectured in ref. 29. This phenomenon appears to be very general, although a global explanation is still lacking.

6. CONCLUDING REMARKS

In this first part, we have introduced and utilized a general representation for describing the linear evolution of perturbations in spatially extended systems. We claim that spatial and temporal spectra allow for a comprehensive description of all phenomena occurring in this framework. In the second part we shall discuss the relationships of the comoving and "rotated" exponents mentioned in the Introduction with SLS and TLS. Furthermore, we shall show that the two latter spectra can be derived from a single "potential," so that an even more compact representation of linear-stability properties exists.

ACKNOWLEDGMENTS

We thank Giovanni Giacomelli, Peter Grassberger, Holger Kantz, and Arkady Pikovsky for useful discussions. A.T. gratefully acknowledges the European Economic Community for the research fellowship No. ERBCHBICT941569 "Multifractal Analysis of Spatio-Temporal Chaos".

REFERENCES

1. D. Ruelle and J.-P. Eckmann, *Rev. Mod. Phys.* **57**:617 (1985).
2. P. Mannneville, *Dissipative Structures and Weak Turbulence* (Academic Press, San Diego, 1990).
3. A. Politi and A. Torcini, *Chaos*, **2**:293 (1992).
4. G. Giacomelli and A. Politi, *Europhys. Lett.* **15**:387 (1991).
5. R. J. Deissler and K. Kaneko, *Phys. Lett. A* **119**:397 (1987).
6. A. S. Pikovsky, *Chaos* **3**:225 (1993).
7. G. Giacomelli, S. Lepri, and A. Politi, *Phys. Rev. E* **51**:3939 (1995).
8. S. Lepri, A. Politi, and A. Torcini, Chronotopic Lyapunov analysis: (II) Towards a unified approach, unpublished.
9. S. Isola, A. Politi, S. Ruffo, and A. Torcini, *Phys. Lett. A* **143**:365 (1990).
10. K. Kaneko, *Prog. Theor. Phys.* **72**:980 (1984).
11. I. Waller and R. Kapral, *Phys. Rev. A* **30**:2047 (1984).
12. H. Kantz and P. Grassberger, *Phys. Lett. A* **123**:437 (1987).
13. M. S. Bourzutschky and M. C. Cross, *Chaos* **2**:173 (1992).
14. A. S. Pikovsky, *Phys. Lett.* **137A**:121 (1989).

15. Y. Pomeau, A. Pumir, and P. Pelce, *J. Stat. Phys.* **37**:39 (1984); K. Kaneko, *Prog. Theor. Phys.* **74**:1033 (1984); P. Manneville, in *Lectures Notes in Physics*, Vol. 230 (Springer, Berlin, 1985), p. 319; R. Livi, A. Politi, and S. Ruffo, *J. Phys. A* **19**:2033 (1986).
16. J.-P. Eckmann and C. E. Wayne, *J. Stat. Phys.* **50**:853 (1988); Ya. Sinai, A remark concerning the thermodynamic limit of the Lyapunov spectrum, Preprint (1995).
17. P. Grassberger, *Physica Scripta* **40**:346 (1989).
18. I. Shimada and T. Nagashima, *Prog. Theor. Phys.* **61**:1605 (1979); G. Benettin, L. Galgani, A. Giorgilli, and J. M. Strelcyn, *Meccanica* **15**:21 (1980).
19. R. Livi, G. Paladin, S. Ruffo, and A. Vulpiani, In *Advances in Phase Transitions and Disorder Phenomena*, G. Busiello, L. De Cesare, F. Mancini, and M. Marinaro, eds. (World Scientific, Singapore, 1987).
20. K. Kaneko, *Physica* **23D**:436 (1986).
21. E. Abrahams, P. W. Anderson, D. C. Licciardello, and T. V. Ramakrishnan, *Phys. Rev. Lett.* **42**:673 (1979).
22. T. Konishi and K. Kaneko, *Phys. Rev. A* **40**:6130 (1989); *J. Phys. A* **23**:L715 (1990).
23. J. L. Pichard and G. André, *Europhys. Lett.* **2**:477 (1986).
24. S. Lepri, A. Politi, and A. Torcini, Fractal features of Lyapunov vectors, unpublished.
25. F. Izrailev, T. Kottos, A. Politi, and S. Ruffo, unpublished.
26. H. A. Posch and W. G. Hoover, *Phys. Rev. A* **38**:473 (1988).
27. A. S. Pikovsky and J. Kurths, *Phys. Rev. E* **49**:898 (1994).
28. M. Kardar, G. Parisi, and Y. C. Zhang, *Phys. Rev. Lett.* **56**:889 (1986).
29. T. Bohr, G. Grinstein, and C. Jayaprakash, *Chaos* **5**:412 (1994).